ANNALI DI GEOFISICA, VOL. XXXVII, N. 6, December 1994

Transient stresses at Parkfield, California, produced by the *M* 7.4 Landers earthquake of June 28, 1992: implications for the time-dependence of fault friction

Paul Spudich ([1]), **Lee K. Steck** ([2]), **Margaret Hellweg** ([1]), **Jon B. Fletcher** ([1]) **and Lawrence M. Baker** ([1])
([1]) *U.S. Geological Survey, Menlo Park, CA, U.S.A.*
([2]) *Los Alamos National Laboratory, Los Alamos, NM, U.S.A.*

Abstract
The *M* 7.4 Landers earthquake triggered widespread seismicity in the Western U.S. Because the transient dynamic stresses induced at regional distances by the Landers surface waves are much larger than the expected static stresses, the magnitude and the characteristics of the dynamic stresses may bear upon the earthquake triggering mechanism. The Landers earthquake was recorded on the UPSAR array, a group of 14 triaxial accelerometers located within a 1-square-km region 10 km southwest of the town of Parkfield, California, 412 km northwest of the Landers epicenter. We used a standard geodetic inversion procedure to determine the surface strain and stress tensors as functions of time from the observed dynamic displacements. Peak dynamic strains and stresses at the Earth's surface are about 7 microstrain and 0.035 MPa, respectively, and they have a flat amplitude spectrum between 2 s and 15 s period. These stresses agree well with stresses predicted from a simple rule of thumb based upon the ground velocity spectrum observed at a single station. Peak stresses ranged from about 0.035 MPa at the surface to about 0.12 MPa between 2 and 14 km depth, with the sharp increase of stress away from the surface resulting from the rapid increase of rigidity with depth and from the influence of surface wave mode shapes. Comparison of Landers-induced static and dynamic stresses at the hypocenter of the Big Bear aftershock provides a clear example that faults are stronger on time scales of tens of seconds than on time scales of hours or longer.

Key words *stress – surface waves – Parkfield – Landers earthquake*

1. Introduction

The *M* 7.4 Landers earthquake triggered widespread seismicity in the western U.S. (Hill *et al.*, 1993; Anderson *et al.*, 1994) that persisted for at least a month after the Landers event. In some regions the first triggered seismic event occurred more than 12 hours after the Landers earthquake, but the first triggered earthquakes in Long Valley, California, and in The Geysers occurred during the passage of the large-amplitude Love (*Lg*) and Rayleigh (*Rg*) surface wave trains. There is considerable disagreement on the causes, characteristics, and tectonic setting of the triggered events. Hill *et al.* (1993) report that the triggered earthquakes tended to occur in volcanic or geothermal regions typically having strike-slip and normal faulting. They further used a simple relationship to estimate the dynamic

stresses associated with the Landers surface waves, and they showed that the surface waves caused transient stresses much larger than the static stresses predicted by the linear elastic response of a half space model of the Earth to the permanent slip of the fault. Hill *et al.* (1993) speculate that some unknown nonlinear interaction between crustal fluids and the transient seismic stresses was a cause of the triggered seismicity. Anderson *et al.* (1994) showed that numerous triggered earthquakes in Eastern California and Western Nevada did not occur in geothermal or volcanic areas. They hypothesized that the cause of triggering was long period dynamic strains that exceeded some regional threshold value.

Curiously, no triggered seismicity was observed at Parkfield or anywhere else on the San Andreas fault system (Hill *et al.*, 1993), although portions of this system were undoubtedly subjected to large dynamic and static stresses induced by Landers. In this paper we seek to compare the dynamic stresses at a San Andreas site where we have good data, Parkfield, with those stresses experienced at the site of the Big Bear earthquake, in order to determine what characteristics of the dynamic stresses, if any, are responsible for triggering earthquakes. We observed the Landers earthquake using the UPSAR array (Fletcher *et al.*, 1992), a group of 14 triaxial accelerometers located within a 1-square-km region 10 km southwest of the town of Parkfield, California, 412 km northwest of the Landers epicenter (fig. 1). Because of the density of seismic stations in the array, we are able to invert the observed ground motions to determine the interstation strains (and hence stresses) caused by the passage of the Landers surface waves, as will be described in more detail below.

The main goals of this paper are: 1) to invert observed motions to determine surface strain and stress tensors as functions of time and frequency; 2) to develop an improved rule-of-thumb that can be used to estimate dynamic stresses from ground velocity records; 3) to determine the depth-dependence of the observed dynamic stresses; 4) to relate relative sizes of the various stress tensor elements to the observed strike-slip and normal mechanisms of

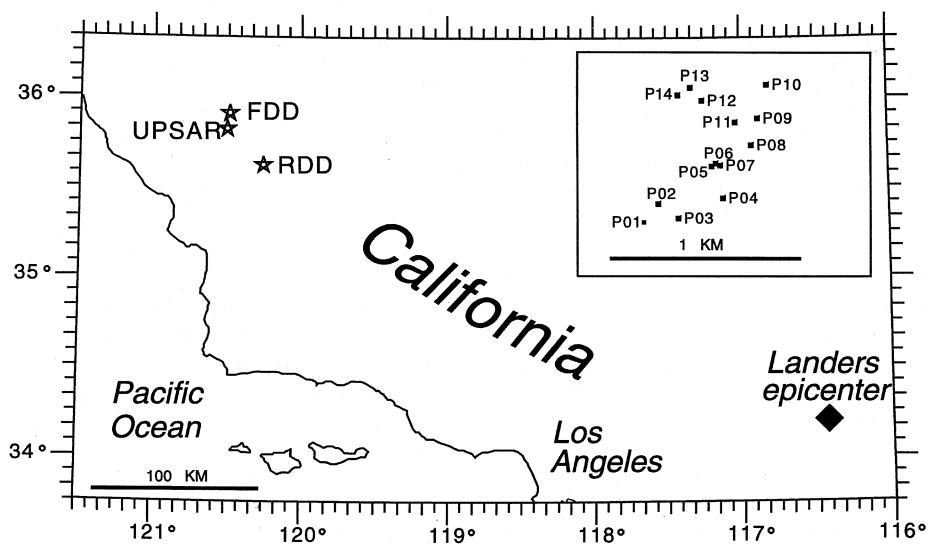

Fig. 1. Study area. Diamond shows epicenter of Landers main shock. Star shows location of UPSAR seismograph array. FDD and RDD are dilatometers. Inset: map of layout of UPSAR array.

the triggered seismicity; 5) to use our understanding of dynamic stresses to examine the time dependence of fault friction on faults near the Landers epicenter.

2. Observations

The Landers earthquake was recorded by all UPSAR stations except P03, P04, P05, and P12, generating a peak acceleration of about 0.01 g on the acceleration channels and clipping the velocity channels. The accelerometers were Kinemetrics FBA-13 force-balance accelerometers, and their outputs were digitized at 200 samples/s per channel using a 16-bit a/d converter having full scale set to 2 g. All array stations are sampled simultaneously (± 0.0001 s). Further details of the instrumentation are given in Fletcher *et al.* (1992). The digitized accelerations were double-integrated to obtain displacement, and they were high-pass filtered at 20 s with an eighth-order zero-phase Butterworth filter to suppress long-period integration noise. They were decimated to 10 samples/s after applying an anti-alias filter having a cosine taper from 1 to 2 Hz.

The displacements at Parkfield are dominated by surface waves in the 10-15 s period band (fig. 2), and peak transverse displacements are ± 2 cm. The wave forms are very similar on similarly oriented transducers at all stations, with the largest source of random noise resulting from the amplification of long period noise by the double integration, as can be seen in the difference traces in fig. 2.

Before we can invert the observed displacements to obtain strains and stresses at depth, it is necessary to ensure that the horizontal seismic wavelengths are long enough so that the array spans only a small fraction of a wavelength in the period range of interest, and it is also necessary to determine what mixture of fundamental and higher mode surface waves is present in the data, since the modes' depth dependences differ and affect the inferred stresses at depth. We have applied a moving-window frequency-wavenumber analysis for the slowness determination, and a multiple-filter analysis to identify the predominant modes in the data.

2.1. *Moving window frequency-wavenumber analysis*

We applied the Broad-Band Frequency-Wavenumber method (BBFK) of Nawab *et al.* (1985) to UPSAR seismograms from the Landers earthquake by moving a time window having 20 s duration along the records in steps of 2 s (fig. 3). Azimuthal accuracy of the BBFK method is about ± 10°. The back azimuth of arrivals at UPSAR shows some evidence of scattering from the Sierra Nevada. The expected azimuth of all Landers phases is 115°. Analyzing displacement records we find that for the first 100 s, Rayleigh and Love waves are arriving from an azimuth of about 120°, consistent with the expected azimuth. However, about 205-225 s after the initiation of the record, waves from a more northerly azimuth are observed. These arrivals have a stable back azimuth of about 70° on the north component. We believe these waves are surface waves scattered or refracted from the Sierra Nevada, a phenomenon which has been observed in other regions of California by Bolt *et al.* (1989) and has been modeled by Tanimoto (1990).

By considering the phase velocities of the Landers surface waves, we can show that for periods of 2 s or greater the array spans a small fraction of a seismic wavelength, justifying the assumption of uniform strain across the array. Phase velocity is poorly resolved by the UPSAR array for the Landers earthquake owing to the small aperture of the array. However, during the largest motions on the north component (90-160 s) phase velocity appears to drop from about 5 km/s to about 3 km/s. Phase velocity behavior is not so simple on the vertical component during the large ground displacements, but it is in the 2-5 km/s range. Similar phase velocities characterize the higher frequency (velocity, acceleration) large motions. Consequently, the horizontal wavelength of a 2 s period wave would be at least 4 km, which is 8 times the extent of the UPSAR ar-

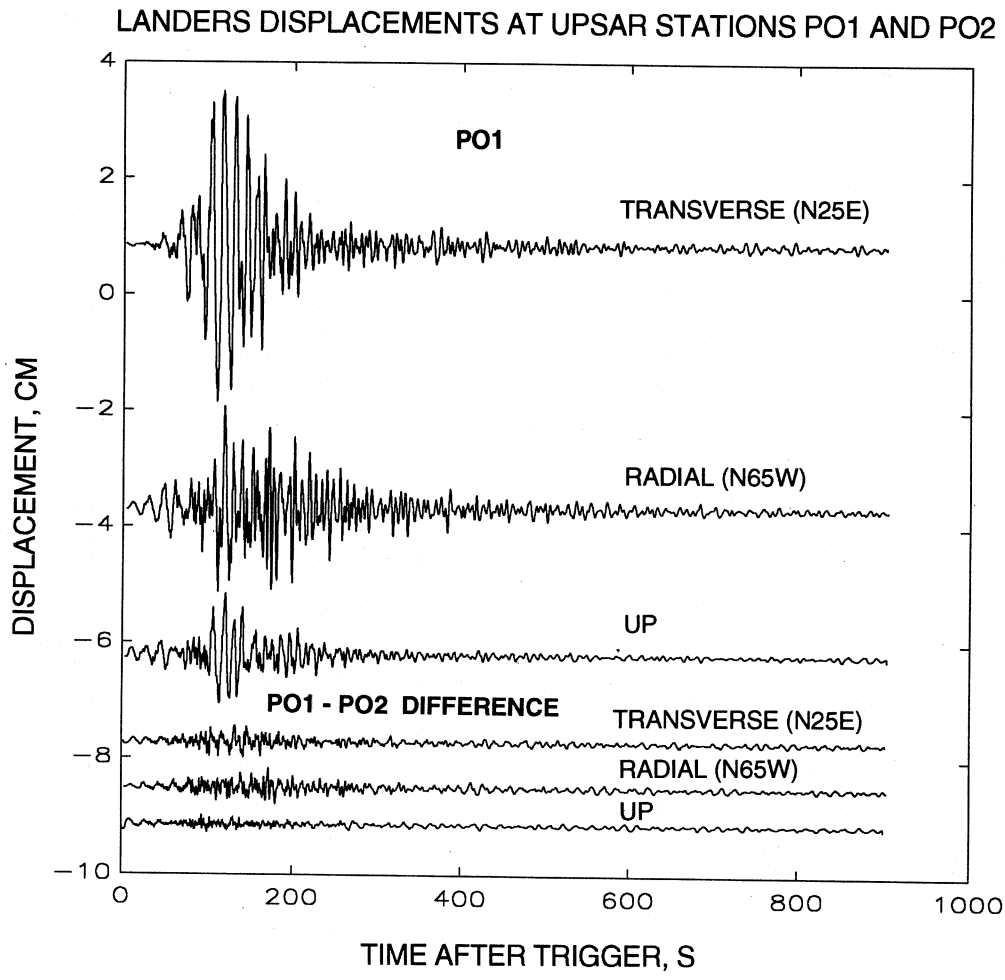

Fig. 2. Upper three traces are transverse, radial, and vertical components of displacement observed at station P01. Lower three traces are differences of displacements between stations P01 and P02, which are separated by 119 m. This difference is an estimate of the noise level.

ray parallel to the phase propagation direction. The observed phase velocities may be biased slightly high, perhaps owing to the averaging properties of the BBFK method. If we choose 1.5 km/s as a reasonable lower limit to phase velocity, then a 2 s period wave has a horizontal wavelength of 3 km, which is 6 times the extent of the UPSAR array parallel to the phase propagation direction.

2.2. *Multiple filter analysis*

To determine group velocity and mode composition of the observed surface waves, we apply the Multiple Filter Analysis technique of Dziewonski *et al.* (1969) (fig. 4). We examined theoretical dispersion curves for several California crustal models in order to fit our group velocity dispersion data and to help identify

the various modes present. A reasonable fit was obtained with an eastern San Andreas model in the vicinity of Parkfield, based on the travel-time inversion results of Michael and Eberhart-Phillips (1991). Dispersion curves for this model overlay the observed curves in fig. 4. It should be noted that since surface waves from Landers propagate through several distinct tectonic provinces, the observed group velocities will be a weighted average of velocities from each province, so the theoretical dispersion curves provide only a rough guide for identifying modes. For both Rayleigh and Love waves we find that the fundamental mode is the dominant signal for periods greater than about 8 s. Below 8 s, the fundamental and first harmonic have similar amplitudes. Scattered energy is also present below 8 s.

3. Determination of surface strains, rotations, and stresses

Given the observed displacements of each seismic station as a function of time, for every time step we perform a fairly standard geodetic inversion to determine the best-fitting uniform surface strain, rotation, and stress tensors.

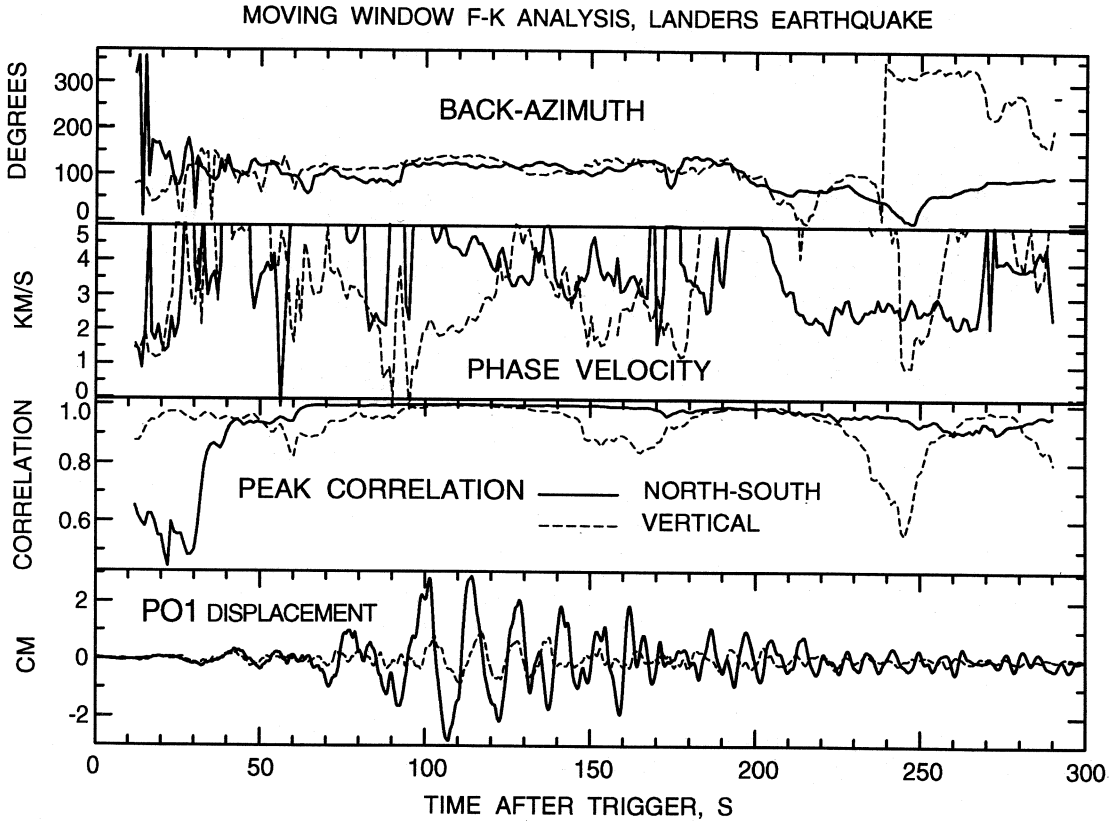

Fig. 3. Moving window frequency-wavenumber analysis of vertical and north components of displacement at UPSAR. A 20 s duration window was moved in increments of 2 s. Back azimuth is the angle clockwise from north toward the apparent source of the waves. Solid lines are results for the north component; dashed lines are for the vertical component. The north component is roughly tangential to the Landers earthquake epicenter.

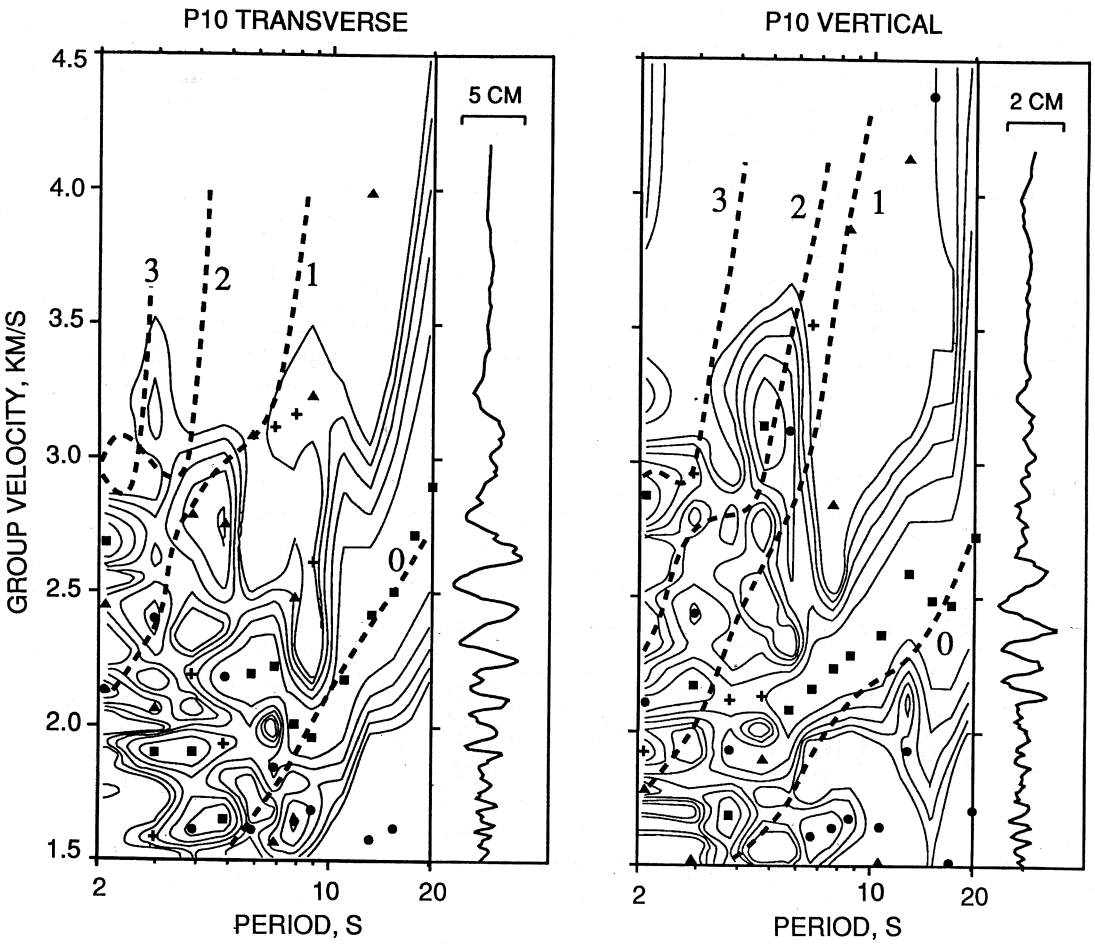

Fig. 4. Multiple filter analysis of transverse and vertical displacements at UPSAR station P10. Contours show amplitude of filter outputs. Dashed lines indicate the predicted group velocity dispersion curves of the fundamental and first three higher modes in the Parkfield east structure. Squares, circles, triangles, and crosses indicate respectively the first, second, third, and fourth highest peaks at each period analyzed. To the right of each contour plot is the observed displacement seismogram, shown as a function of group velocity.

Finding a uniform rotation tensor is equivalent to finding the best-fitting rigid body rotation of the entire array about station P01. The method is summarized in appendix A of Spudich *et al.* (1995). The crucial assumption of the inversion is that the strain tensor is spatially uniform in the material under the array. This assumption is probably good for periods greater than 2 or 3 s, because for those periods the associated wavelengths are considerably larger than the array dimension.

Peak strains at the array are in the range 5-10 microstrain, and peak rotations are about 6 microradians (fig. 5). Both time series are large when the displacements are large, indicating that there are observable strains and rotations associated with the surface wave train. In order to quantify the fraction of the data that

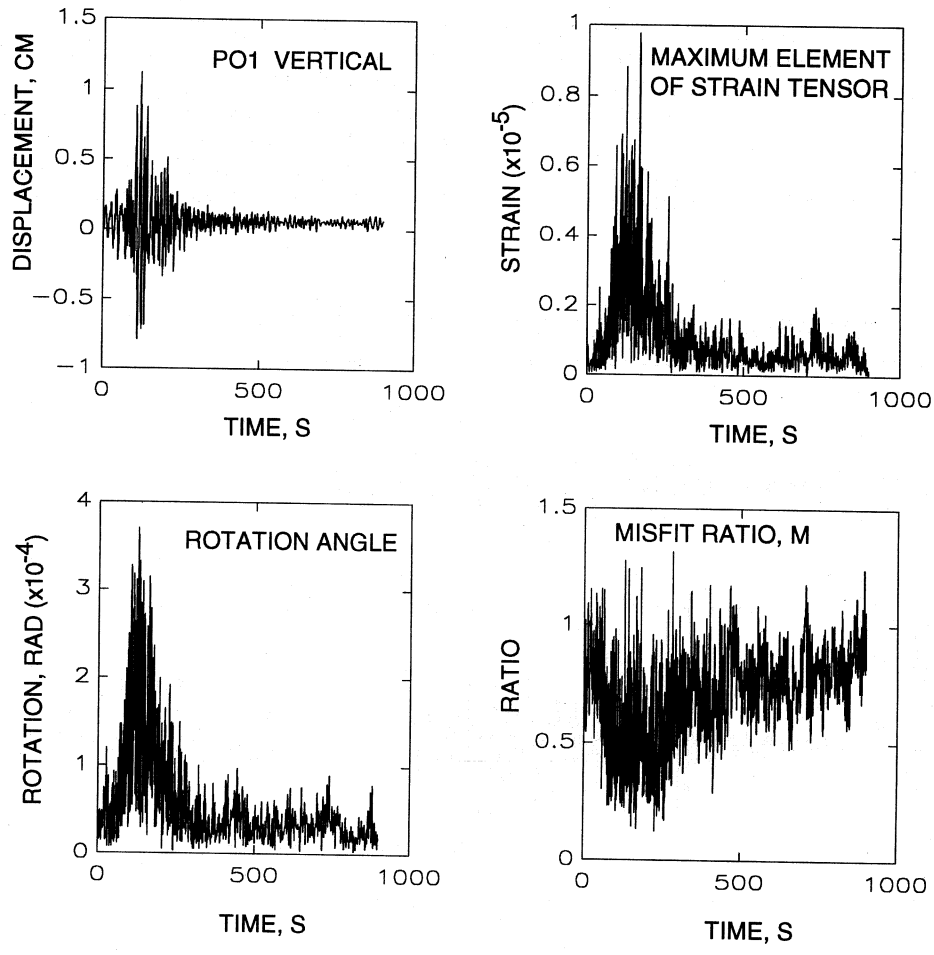

Fig. 5. Results of inversion of observed displacements of the array stations. Upper left: P01 vertical displacements. Upper right: maximum absolute value of any element of the inferred uniform strain tensor. Lower left: absolute value of best fitting rigid body rotation of array about P01. Lower right: misfit ratio M, showing proportion of total array station displacements not explained by a uniform rotation and strain (see appendix A of Spudich *et al.*, 1995).

is not satisfied by our assumption of uniform strain and rotation, we have concocted a measure M that we call the «misfit ratio». To calculate M we first calculate the misfit vectors, which are the difference vectors between observed and predicted station displacement vectors. M is the ratio of the summed lengths of the misfit vectors over the summed lengths of the data vectors. See Spudich *et al.* (1995) for details. The misfit ratio drops to about 0.5 during the strong shaking, and is close to 1 during the coda from 500 s to 900 s. A misfit ratio of 0.5 means that about half of the total displacement differences between stations is being explained by a uniform strain and a rigid body rotation about station P01.

It is especially interesting to examine the inferred dilatational strain because two indepen-

dent records of dilatational strain during the Landers event are available from the Parkfield region (M.J.S. Johnston, unpublished data, 1992). Comparison of these records with the UPSAR inferred dilatation confirms that the inversion method is producing reasonable results, at least in the 18-5 s period range. Figure 6 shows dilatometer records from RDD and FDD, approximately 31 km southeast and 11 km north of UPSAR, respectively (fig. 1). The unfiltered dilatometer records look rather different from the UPSAR dilatational strain, but when both sets of records are band-pass filtered in the 18-5 s band, there is obvious wave

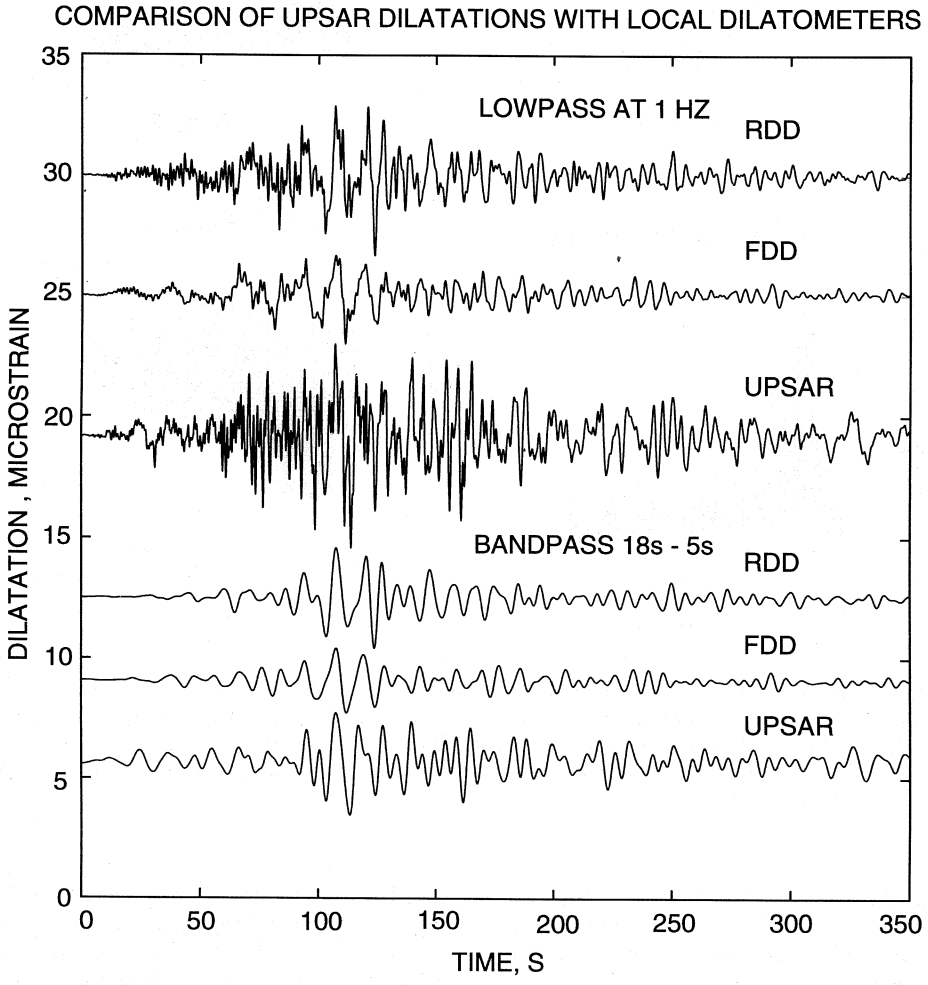

Fig. 6. Dilatational component of strain tensor inferred from UPSAR displacements compared with locally observed dilatations recorded at RDD and FDD (fig. 1). Upper three records: dilatations low pass filtered at 1 Hz. Lower three traces: dilatations band-pass filtered from 18 s to 5 s period. The UPSAR band passed dilatation agrees reasonably well with the other records, although the UPSAR record has more noise at late times.

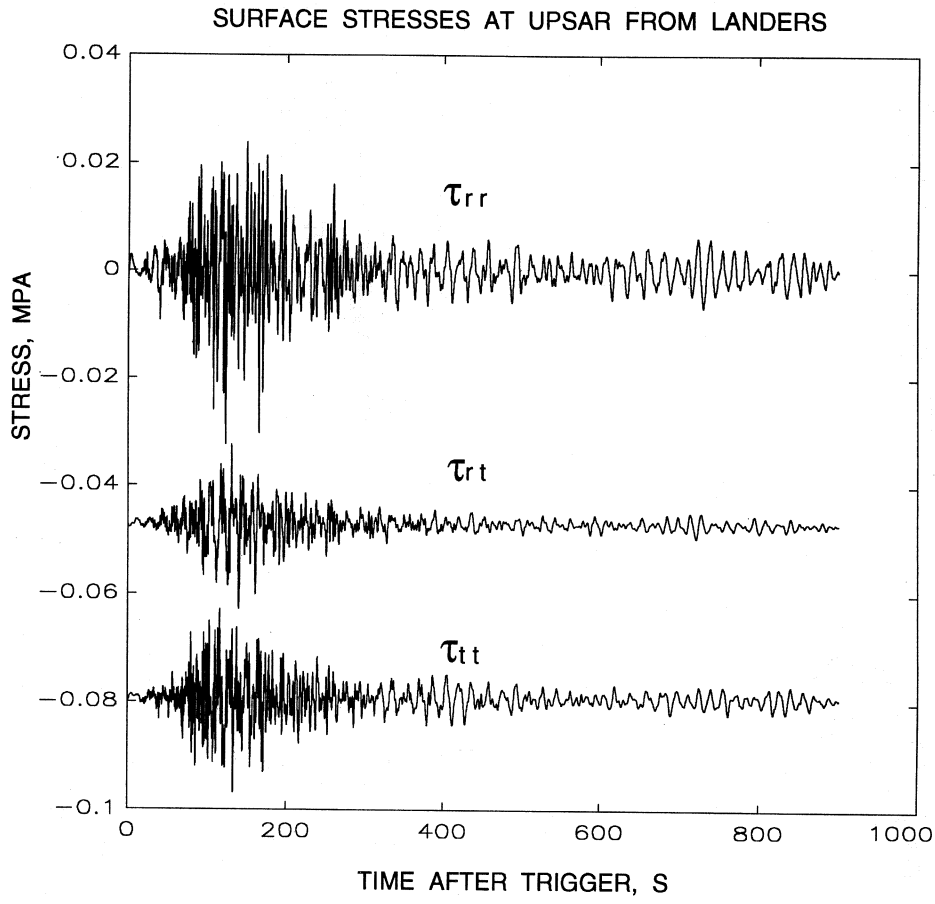

Fig. 7. The 3 nonzero components of stress at the Earth's surface, as inferred from UPSAR displacement recordings of the Landers earthquake. Time series after 600 s are dominated by integration noise.

form coherence during the strong part of the shaking. Because the UPSAR displacements were high-pass filtered at 20 s, they lack the long periods in the dilatometer records. We do not understand why the inferred UPSAR dilatations contain more high frequency energy (periods less than 5 s) than the dilatometer records. The discrepancy might be related to free-surface effects and surface reflections; the UPSAR array sits on the surface of a rather soft deposit, while the dilatometers are emplaced at 200 m depth in a harder material.

3.1. *Surface stresses derived from strain tensor and ground velocity*

Surface stresses are easily derived from the inferred strain tensor, and they have peak values at the surface of 0.015-0.03 MPa for τ_{rr}, τ_{rt}, and τ_{tt}, with all other stress components being zero owing to the free-surface boundary condition (fig. 7). We derived these stresses from the strain tensor using material properties determined by Gibbs and Roth (1989) for the Paso Robles formation, upon which UPSAR

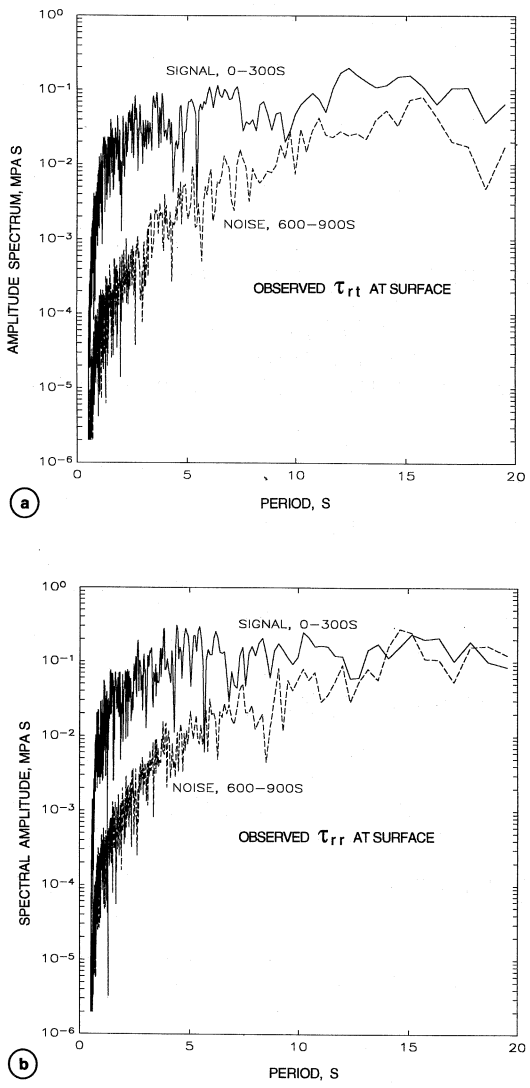

Fig. 8a-c. Comparison of nominal signal and noise spectra for the three surface stress components. The first 300 s of the stress time series are taken to be the signal (actually, signal + noise), and the sections of the stress time series from 600-900 s after the initiation of the record are assumed to be the noise. The true noise level is less than this, but probably not much less. All time series had the beginning and ending 10% cosine tapered. a) τ_{rt}. S/N ratio is greater than 2 throughout the entire period band of interest. b) τ_{rr}. There is essentially no signal for periods longer than 12 s. c) τ_{tt}. There is essentially no signal for periods longer than 13 s.

sits. From their work we estimated P and S velocities of 1.45 km/s and 0.72 km/s, respectively, and a density of 2.3 Mg/m^3 for a depth of 100 m. Note that our surface stresses are an underestimate of the stresses at depth, owing to a factor of 20 rise in rigidity going from the surface to the midcrust. We will estimate stresses at depth later in this paper.

Although the ground displacements are dominated by surface waves having 10 s to 15 s period, the spectra of the stresses are fairly flat from 2 s to 15 s (fig. 8a-c). As an estimate of the noise level, we used the coda portions of the stress time series from 600 s to 900 s after the trigger, which are certainly an upper bound on the noise. Figure 8a-c shows that the τ_{rt} component has the largest signal-to-noise ratio of the three stress components at periods from 10 s to 15 s, which will be important when we discuss rules-of-thumb. We believe that the

600 s to 900 s portion of the coda is a good representative of the noise in the inferred stresses because the misfit ratio in fig. 5 is almost unity in the coda, which is the value that would be expected for uncorrelated noise used as data (see appendix A of Spudich *et al.*, 1995). In addition, we verified by numerical experiments that the spectrum of the coda is consistent with the spectrum of the stresses that would be inferred from data seismograms having errors consistent with the displacement differences of stations very close to each other, such as those shown in fig. 2. Consequently, our array determination of long period stresses is corrupted by the high long-period noise levels introduced by double integration of the rather small accelerograms to displacement.

We can alternately estimate the three components of the surface stress tensor spectrum by using a simple, approximate relationship in which the ground strain is obtained from ground velocity by dividing ground velocity by the surface wave phase velocity (see appendix B of Spudich *et al.*, 1995). We have integrated the observed accelerations to obtain ground velocity. Surprisingly, surface stresses estimated from ground velocities are as good, if not better, than stresses estimated from our array measurements of displacements. The stresses are estimated from spatial differences of doubly integrated accelerograms, and presumably these stresses have greater error at long periods than do the velocities, which are singly integrated accelerograms. Figure 9 shows a comparison of the stress spectra from array measurements (from fig. 8a-c) and spectra determined using velocity records (using eq. B3 and B6 from appendix B of Spudich *et al.* (1995) and assuming that the observed ground velocities consist of only fundamental modes). Rayleigh wave stresses τ_{rr} and τ_{tt} were estimated using the radial component of ground velocity, because the radial component was larger than the vertical component, and also because the inference of surface stress from radial velocity is slightly simpler than from vertical velocity (appendix B of Spudich *et al.*, 1995).

The agreement in fig. 9 of the two methods for Love wave stress τ_{rt} is astonishingly good over the entire spectral band from 20 s to 1 s period. At periods longer than 10 s, the array method yields estimates of τ_{rt} that are about 50% higher than those obtained from velocity records. However, fig. 8a-c shows that the array measurement of τ_{rt} may be biased high because of a significant noise contribution. We note that the agreement of the spectral levels for periods shorter than 10 s depends upon using the fundamental Love wave phase velocity curve. Between 20 s and 1 s period the Love wave phase velocity drops from about 4.5 km/s to about 1.5 km/s. If we chose to use an average phase velocity of 2.5 km/s over the entire period range, we would introduce an error less than a factor of 2, which might still be adequately accurate for some uses.

The two methods agree reasonably well for Rayleigh wave stresses τ_{rr} and τ_{tt}, and again the stresses determined from ground velocities are probably more accurate. For τ_{rr} in the period range shorter than 12 s, both methods agree well, but for longer periods, the array measurements of stress substantially exceed those inferred from radial ground velocities. However, fig. 8a-c shows that the array measurement of τ_{rr} is corrupted by noise for periods longer than 12 s, once again suggesting that the stress spectral levels determined by array measurement are overestimates of the true spectral level. For τ_{tt} the situation is not so clear. While in fig. 8a-c for τ_{tt} the signal far exceeds the noise in the 9-13 s band, the array measurement of τ_{tt} exceeds that derived from the radial ground velocity in the same band. Perhaps the particular noise sample used in fig. 8a-c happened to be deficient in the 9-13 s band.

3.2. *Inference of stresses at depth*

We estimated stresses at depth by multiplying surface stress spectra by theoretical ratios derived from the Parkfield velocity structure relating surface and deep stresses. Specifically, we used (B9) of Spudich *et al.* (1995) and analogous relations for other stress tensor elements, with the simplifying approximation that the first higher mode phase velocity equaled

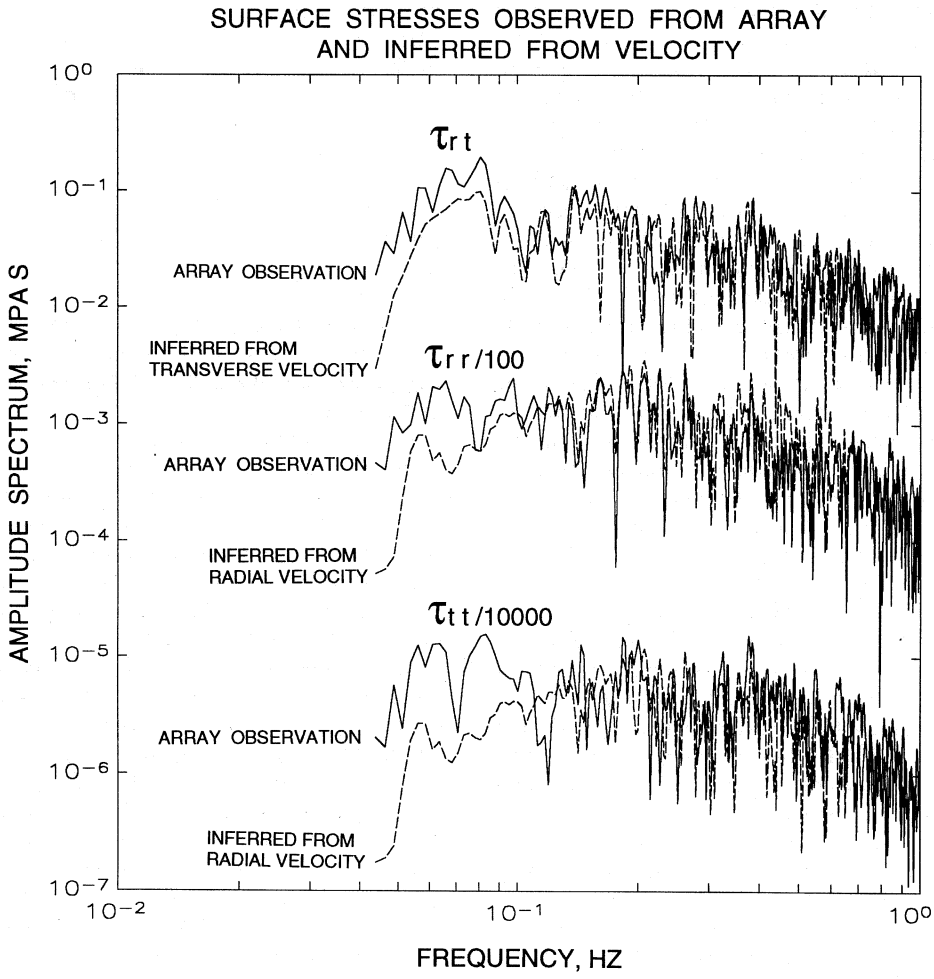

Fig. 9. Comparison of stresses determined from inversion of UPSAR surface displacements (observed) with stresses inferred from the ground velocity records scaled by the phase velocity. The *rr* and *tt* components of stress have been shifted vertically by the indicated factors for clarity. Note that for all components of the stress tensor, the observed value is larger than the inferred value for periods longer than 10 s, although the spectra agree extremely well for shorter periods.

that of the fundamental mode. This approximation causes an error less than a factor of 2 at worst.

Three main observations can be drawn from the stresses at depth. First, owing to the rapid increase of rigidity with depth at Parkfield, stresses increase very rapidly with depth in the top few km of the crust, rising to values about a factor of 5 greater than at the surface (fig. 10). These peak stress values were obtained by inverse Fourier transforming the inferred stress spectra and by taking the maximum absolute values of the resulting oscillatory time series. In other regions lacking Parkfield's low surface rigidities, deep stresses will not be so much larger than shallow stresses.

Second, the depth dependences of various stress tensor elements differ considerably from each other, primarily due to the influence of the free-surface boundary condition, which dictates that the *rz*, *tz*, and *zz* components of stress must be zero at the surface. Figure 10 shows that the *zz* and *rz* components of stress grow very slowly with depth, reaching maxima at 10 km depth or greater. In the top 5 km of the crust at Parkfield, the *rr*, *tt*, *rt*, and *tz* components of stress dominate. Note that the first three of these involve horizontal tractions across vertically oriented planes.

Third, at depths greater than 1-2 km the stress spectra are richer in long periods than in short periods (fig. 11). The dominance of longer period stresses at depth, despite the relatively flat stress spectrum at the surface (fig. 8a-c), results from the deeper penetration of the longer period modes.

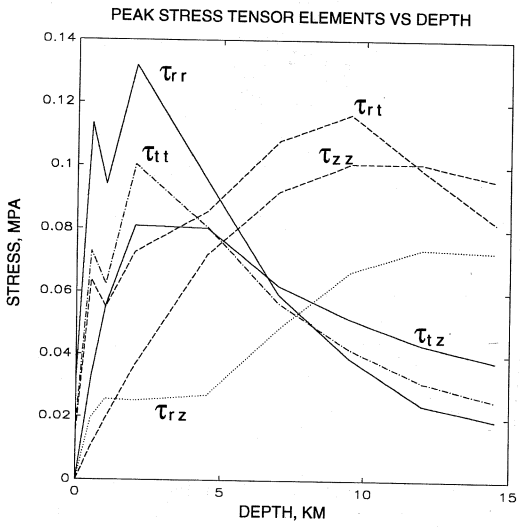

Fig. 10. Peak values of each stress tensor time series as a function of depth in the crust at Parkfield. The *rz*, *tz*, and *zz* components are zero at the surface owing to the free-surface boundary condition. The rapid rise of the stresses with depth in the top 2 km is due to the rapid increase of rigidity with depth. Stresses associated with horizontally oriented tractions on vertical planes predominate in the top 5-6 km, perhaps accounting for the triggered strike-slip activity.

4. Discussion

The fact that the Landers earthquake preferentially triggered seismicity in regions previously having strike-slip and normal faulting events (Hill *et al.*, 1993) may be related to the depth dependence of the dynamic stress tensor elements (fig. 10). We observe that for depths shallower than about 5 or 6 km, the *rr*, *tt*, *rt*, and *tz* components of stress predominate, and at greater depths the terms involving *z* derivatives become larger. As the *rr*, *tt*, *rt*, and *tz* components mostly involve tractions acting across vertical planes, this stress system would tend to favor faulting across vertical or near-vertical planes in the top 5 or 6 km at Parkfield. Other mechanisms would be expected at greater depths.

If the triggered seismicity changes mechanism with depth, having more horizontally oriented fault planes at greater depths, then this would tend to indicate that the dynamic stresses trigger seismicity by direct working and weakening of materials in suitably oriented pre-existing fault structures. If there is no change of mechanism with depth, then the dynamic stresses may be acting by some indirect method, such as by affecting fluid flow in the crust. Alternately, a lack of mechanism change might indicate that the focal mechanisms of the triggered seismicity are dominated by the pre-existing tectonic stress. Although at Parkfield we postulate that the orientation of dynamic stresses changes at about 5-6 km depth, this transition might occur at a different depth, perhaps even beneath the seismogenic zone, in some other crustal structure.

In order to compare our dynamic stress changes with the static stress changes observed by others, we estimate the dynamic change in stress for Coulomb failure at Parkfield. Using the definition of Stein *et al.* (1992) we estimate peak values of the dynamic changes in stress for Coulomb failure to be about 0.08-0.14 MPa, resulting from simultaneous shear

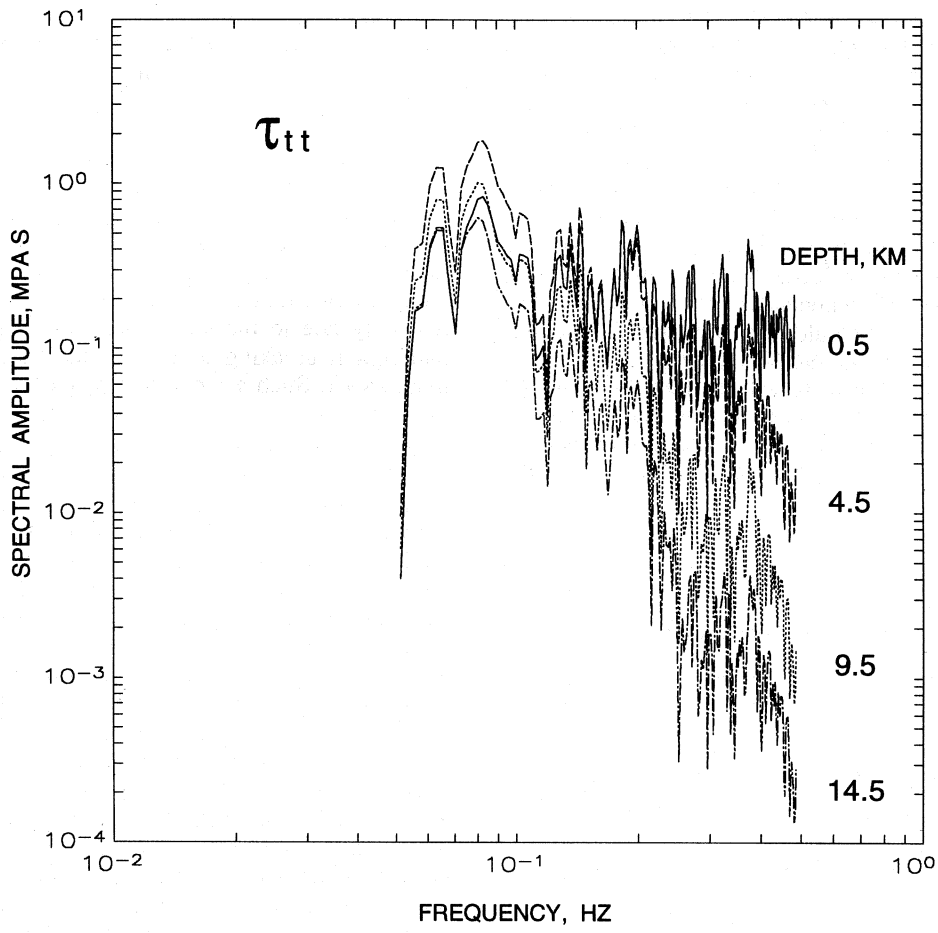

Fig. 11. Spectra of the *tt* component of stress at 0.5, 4.5, 9.5, and 14.5 km depth. The stress spectrum is fairly flat at the surface, but long period motions dominate the stresses at greater depths.

stresses and normal dilatational stresses of about 0.08 MPa (fig. 10) and allowing the frictional coefficient μ' of Stein *et al.* (1992) to range between 0.0 and 0.75. In this estimate we assume that the maximum shear stress and dilatation are simultaneous for the following reason. The *rr* and *tt* components of stress are in phase with each other and are associated with Rayleigh waves (appendix B of Spudich *et al.*, 1995); these components would exert compression or dilation, rather than shearing, on any vertical fault plane. The *rt* and *tz* components are associated with Love waves and probably would have no fixed phase relationship with the compressions and rarefactions caused by the Rayleigh waves, owing to the differing dispersion curves of the two wave types. Consequently, the *rt* and *tz* shears might sometimes coincide with rarefactions caused by the *rr* and *tt* stresses, which is what we assume in the above estimate.

If the Coulomb failure criterion actually governs the triggering of earthquakes, then our work, when combined with that of others,

strongly implies that the strength of faults must be time dependent, in that small changes in stress acting over a period of hours to weeks seem to be more correlated with the occurrence of tectonic earthquakes than are large stress changes acting on periods of seconds. Specifically, Stein *et al.* (1992) have correlated the triggering of the Big Bear aftershock of the Landers earthquake with a 0.3 MPa change in Coulomb failure stress caused by Landers at the Big Bear hypocenter, about 40 km distant. The dynamic Coulomb failure stresses caused by the Landers earthquake at the Big Bear hypocenter must have far exceeded the 0.3 MPa static stress change, because we have observed a 0.1 MPa dynamic stress change at Parkfield, 400 km from Landers. We can estimate that dynamic stresses at the Big Bear hypocenter may have been 1-2 MPa, using the simple relationship of Hill *et al.* (1993) and the peak ground velocities estimated by Wald and Heaton (1994) (fig. 12). This raises the question of why the dynamic stresses from Landers failed to trigger the Big Bear earthquake immediately as those waves passed through the hypocentral region, although the static stresses (apparently) succeeded after a 3.5 h delay. The Big Bear fault, striking northeast, was favorably oriented for the stresses induced by *SH* waves propagating southwestward from Landers. In addition, numerous favorably oriented northwestward striking faults are mapped between the Big Bear region and the Landers source zone, and it is still mysterious that 1-2 MPa of stress on these faults failed to trigger them when 0.3 MPa triggered Big Bear. The simplest interpretation is that faults are much stronger on short time scales (tens of seconds) than on longer time scales (hours or more). We cannot say whether this time dependence is an intrinsic property of rock friction or whether it results from weakening of a fault caused by damage to the fault zone materials. Such weakening might occur if dynamic stresses caused microcracking in the fault zone materials, allowing pore fluids to penetrate the fault zone and raise pore pressure. If we hypothesize that during the 3.5 h between the Landers and Big Bear events, the pore fluid pressure at the Big Bear hypocenter gradually rose until the Coulomb failure function exceeded its peak value during the dynamic shaking from Landers, then the pore fluid pressure would have to have risen by at least 0.7 MPa during that 3.5 h period. This pressure rise is equivalent to a 70 m rise in the water table.

Note that the loss of frictional strength on the Big Bear fault may be occurring by a process different than that causing aftershocks on the primary rupture surface. Fluid pressure on the primary rupture surface must change substantially due to the slip on the fault and the consequent breaking of fluid seals during the main shock. Such a process may not be occurring on other regional faults that do not slip during the main shock.

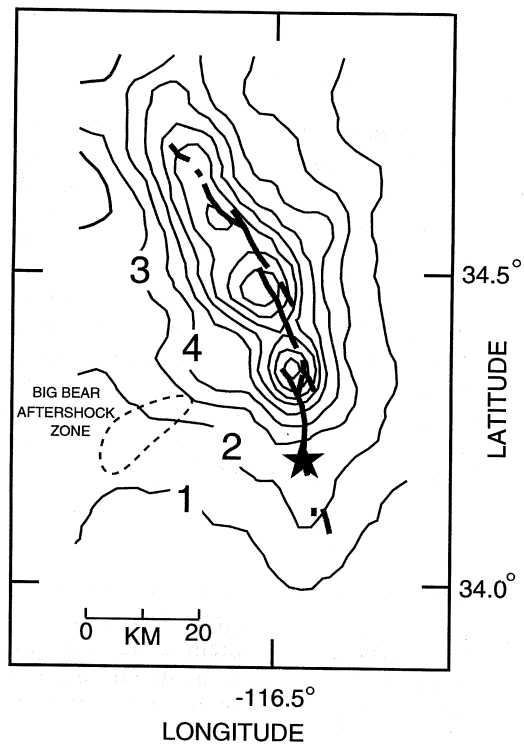

Fig. 12. Predicted peak dynamic shear stresses in the Landers region, derived from the peak velocity map of Wald and Heaton (1994) and the approximate relation 1 cm/s = 0.1 MPa. Star shows Landers earthquake epicenter, gray line shows surface fault rupture.

Unfortunately, we cannot determine whether the dynamic stresses experienced in the Parkfield region will have any effect on the time of occurrence of the next Parkfield earthquake. The dynamic stresses from Landers are comparable in magnitude to the static stress changes caused on the San Andreas fault by the 1983 Coalinga earthquake (Mavko *et al.*, 1985; Simpson *et al.*, 1988). Those static changes were accompanied by coseismic creep events of about 5 mm amplitude on a few Parkfield area creep meters, and left-lateral creep on creep meter XMM1 for about a year. The Landers event has had no such obvious effects on Parkfield area creep (K. Breckenridge, USGS, unpublished data, 1993), so the Landers earthquake will probably have less of an effect than Coalinga on the timing of the next Parkfield earthquake.

Acknowledgements

Large portions of this manuscript are quoted verbatim from Spudich *et al.* (1995), with permission of the American Geophysical Union. We thank R.B. Herrmann for installing his surface wave codes on our local computer and for helpful comments on the manuscript. We thank M.J.S. Johnston for allowing us to present his unpublished dilatometer records, D.B. Harris for use of his array analysis codes, and J. Dieterich, J. Gomberg, H.M. Iyer, and D.M. Boore for reviews of the manuscript. Use of product names is for descriptive purposes only and does not imply endorsement by the U.S. Geological Survey.

REFERENCES

Anderson, J.G., J.N. Brune, J.N. Louie, Y. Zeng, M. Savage, G. Yu, Q. Chen and D. de Polo (1994): Seismicity in the Western Great Basin apparently triggered by the Landers, California, earthquake, 28 June 1992, *Bull. Seismol. Soc. Am.*, **84**, 863-891.

Bolt, B.A., A. Lomax and R.A. Uhrhammer (1989): Analysis of regional broadband recordings of the 1987 Whittier Narrows, California earthquake, *J. Geophys. Res.*, **94**, 9557-9568.

Dziewonski, A., S. Bloch and M. Landisman (1969): A technique for the analysis of transient seismic signals, *Bull. Seismol. Soc. Am.*, **59**, 427-444.

Fletcher, J.B., L.M. Baker, P. Spudich, P. Goldstein, J.D. Sims and M. Hellweg (1992): The USGS Parkfield, California, dense seismograph array: UPSAR, *Bull. Seismol. Soc. Am.*, **82**, 1041-1070.

Gibbs, J. and E. Roth (1989): Seismic velocities and attenuation from borehole measurements near the Parkfield prediction zone, Central California, *Earthq. Spectra*, **5**, 513-537.

Hill, D.P., P. Reasenberg, A. Michael, W. Arabasz, G. Beroza, D. Brumbaugh, J. Brune, R. Castro, S. Davis, D. de Polo, W. Ellsworth, J. Gomberg, S. Harmsen, L. House, S. Jackson, M. Johnston, L. Jones, R. Keller, S. Malone, L. Munguia, S. Nava, J. Pechmann, A. Sanford, R. Simpson, R. Smith, M. Stark, M. Stickney, A. Vidal, S. Walter, V. Wong and J. Zollweg (1993): Seismicity remotely triggered by the *M* 7.3 Landers, California, earthquake, *Science*, **260**, 1617-1623.

Mavko, G.M., S.S. Schulz and B.D. Brown (1985): Effects of the 1983 Coalinga, California, earthquake on creep along the San Andreas fault, *Bull. Seismol. Soc. Am.*, **75**, 475-489.

Michael, A.J. and D. Eberhart-Phillips (1991): Relations among fault behavior, subsurface geology, and three-dimensional velocity models, *Science*, **253**, 651-654.

Nawab, S.H., F.U. Dowla and R.T. Lacoss (1985): Direction determination of wideband signals, *IEEE Trans. Acoust., Speech, Signal Processing, ASSP-33*, 1114-1122.

Simpson, R.W., S.S. Schulz, L.D. Dietz and R.O. Burford (1988): The response of the creeping parts of the San Andreas fault to earthquakes on nearby faults: two examples, *Pure Appl. Geophys.*, **126**, 665-685.

Spudich, P., L.K. Steck, M. Hellweg, J.B. Fletcher and L.M. Baker (1995): Transient stresses at Parkfield, California, produced by the *M* 7.4 Landers earthquake of June 28, 1992: observations from the UPSAR dense seismograph array, *J. Geophys. Res.* (in press).

Stein, R.S., G.C.P. King and J. Lin (1992): Change in failure stress on the Southern San Andreas fault system caused by the 1993 Magnitude = 7.4 Landers earthquake, *Science*, **258**, 1328-1332.

Tanimoto, T. (1990): Modelling curved surface wave paths: membrane surface wave synthetics, *Geophys. J. Int.*, **102**, 89-100.

Wald, D.J. and T.H. Heaton (1994): Spatial and temporal distribution of slip for the 1992 Landers, California, earthquake, *Bull. Seismol. Soc. Am.*, **84**, 668-691.